

The structure, spectroscopy, and excited state predissociation dynamics of GeH₂

J. Karolczak, Warren W. Harper, Roger S. Grev, and Dennis J. Clouthier

Citation: *The Journal of Chemical Physics* **103**, 2839 (1995); doi: 10.1063/1.470520

View online: <http://dx.doi.org/10.1063/1.470520>

View Table of Contents: <http://scitation.aip.org/content/aip/journal/jcp/103/8?ver=pdfcov>

Published by the [AIP Publishing](#)

Articles you may be interested in

[Microwave spectroscopy of the HCCS and DCCS radicals \(\$\tilde{X}^2\Pi_i\$ \) in excited vibronic states: A study of the Renner–Teller effect](#)

J. Chem. Phys. **105**, 8020 (1996); 10.1063/1.472715

[Ultrafast excitedstate H atom transfer in jetcooled 2\(2'hydroxyphenyl\)oxazole derivatives](#)

AIP Conf. Proc. **364**, 383 (1996); 10.1063/1.50150

[Photoelectron spectroscopy and electronic structure of clusters of the group V elements. III. Tetramers: The \$2T_2\$ and \$2A_1\$ excited states of \$P^+4\$, \$As^+4\$, and \$Sb^+4\$](#)

J. Chem. Phys. **93**, 6327 (1990); 10.1063/1.458975

[Photodissociation of RNCS and RSCN \(R=H, CH₃, C₂H₅\): Evidence for an excited state isomerization and energy deposition in the NCS product](#)

J. Chem. Phys. **93**, 2337 (1990); 10.1063/1.459013

[Theory of chemical reactions of vibronically excited H₂\(\$B^1\Sigma^+_u\$ \). I. Prediction of a strongly bound excited state of H₄](#)

J. Chem. Phys. **80**, 1705 (1984); 10.1063/1.446874



The structure, spectroscopy, and excited state predissociation dynamics of GeH₂

J. Karolczak,^{a)} Warren W. Harper, Roger S. Grev, and Dennis J. Clouthier^{b)}
Department of Chemistry, University of Kentucky, Lexington, Kentucky 40506-0055

(Received 1 May 1995; accepted 17 May 1995)

The spectroscopy and excited state dynamics of \tilde{A}^1B_1 germylene (GeH₂) have been investigated experimentally and theoretically. Jet-cooled laser-induced fluorescence spectra of GeH₂ were obtained by subjecting germane (GeH₄) to an electric discharge at the exit of a pulsed nozzle. The band origins of ten vibronic transitions were determined, giving values for the upper state fundamentals of $\nu_1=783.0\text{ cm}^{-1}$ and $\nu_2=1798.4\text{ cm}^{-1}$. Sufficient numbers of 0_0^0 band rovibronic transitions were observed to give the ground and excited state structures as $r''=1.591(7)\text{ \AA}$, $\theta''=91.2(8)^\circ$ and $r'=1.553(12)\text{ \AA}$, $\theta'=123.4(19)^\circ$. Fluorescence lifetime measurements show that the $0_{0,0}$ rotational levels decay radiatively; higher J rotational states in the 0^0 vibronic level decay much faster, due to a heterogeneous predissociation in the excited state. High quality *ab initio* studies are consistent with a model in which the lower vibronic levels of the \tilde{A} state predissociate through the \tilde{a}^3B_1 state to produce $\text{Ge}(^3P)+\text{H}_2(^1\Sigma_g^+)$. The transition state for this process has been located and the barrier to dissociation is 15.2 kcal/mol above the \tilde{A}^1B_1 state, so that tunneling through the barrier must occur. Above 4000 cm^{-1} of vibrational energy in the \tilde{A} state, a breaking off of fluorescence is observed as a second predissociation channel involving $\text{GeH}_2(\tilde{A}^1B_1)\rightarrow\text{Ge}(^1D)+\text{H}_2(^1\Sigma_g^+)$ becomes accessible. This process is also found to have a barrier, in contrast to previous theoretical studies of SiH₂, where the analogous dissociation was predicted to be barrierless. © 1995 American Institute of Physics.

I. INTRODUCTION

The production of semiconductors involving Si/Ge alloys or heterostructures has received considerable attention in recent years. These systems have great potential for the fabrication of electronic devices, because they offer the possibility for band gap engineering through modifications of the stoichiometry or growth patterns.^{1,2} The primary method for growing such structures is chemical vapor deposition (CVD), in which feed gases (SiH₄, GeH₄, etc.) flow over the heated substrate surface in vacuum, depositing thin layers of silicon and/or germanium of the desired composition. The low temperature growth of germanium films by laser photodissociation of GeH₄ on or near the substrate surface has also been investigated as a way of producing more carefully controlled deposition.²⁻⁴ In addition, laser processes have the potential for direct writing of circuit elements onto surfaces. Other techniques for growing germanium films include molecular beam epitaxy^{5,6} and various electric discharge methods.⁷⁻⁹

Silanes, germanes, and their halogen-substituted analogs are the most common precursors used in the chemical vapor deposition of silicon and germanium. As pointed out by Lu and Crowell¹⁰ in 1993, "although the chemical vapor deposition of Si or Ge from these gases is well-established technology, the mechanistic details are far from well understood." In the case of germanium, germylene (GeH₂) has often been cited as a reactive intermediate in these processes. For example, studies of the thermal decomposition of ger-

mane in the gas phase show that the initial process is the production of GeH₂ and H₂.¹¹ GeH₂ has been postulated as the primary precursor in the germane laser-assisted chemical vapor deposition process and a model has been developed for the subsequent film growth.¹² GeH₂ and GeH₃ have been detected by infrared absorption spectroscopy of the matrix-isolated products of a low-pressure dc discharge through germane.¹³ In studies of the interaction of digermane with germanium surfaces, infrared spectroscopy revealed the presence of GeH₃, GeH₂, and GeH in varying quantities at different temperatures.¹⁴ The interaction of diethylgermane with Si surfaces, as characterized by photoelectron spectroscopy, also revealed GeH₂ as a major surface adsorption product.¹

One of the major impediments to ascertaining the importance of gas phase GeH₂ in semiconductor growth processes is the lack of a sensitive spectroscopic method for detecting and quantifying it. Indeed, it is astonishing how little is known about germylene, considering the importance of germanium hydrides in semiconductor processing and the extensive research activity on the corresponding carbene and silylene species. Until recently, the only available spectroscopic data were the ground state vibrational frequencies, obtained in 1972 from matrix isolation studies¹⁵ of the photolysis of GeH₄. The gas phase microwave, infrared and photoelectron spectra are unknown. In 1993, Saito and Obi reported the laser-induced fluorescence (LIF) spectra of GeH₂ and GeD₂, produced by the photolysis of phenylgermane in a supersonic free jet expansion.^{16,17} They observed five vibronic bands for each species (2_0^n , $n=0-4$), in the 612-514 nm region. Each band consisted primarily of a transition to the lowest rotational level in the upper state, sug-

^{a)}Permanent address: Quantum Electronics Laboratory, Institute of Physics, A. Mickiewicz University, Grunwaldzka 6, 60-780 Poznan, Poland.

^{b)}Author to whom correspondence should be addressed.

gesting an excited state predissociation process similar to that in SiH₂. The authors obtained the harmonic bending frequencies and x_{22}^0 anharmonicity constants for the ground and excited states. While the present work was in progress, Saito and Obi published a further study¹⁸ in which they measured fluorescence lifetimes of the excited state levels, observed the 2_0^5 and 2_0^6 bands of GeD₂ and postulated a mechanism for the predissociation process. By analogy with SiH₂,¹⁹ they suggested that the S_1 excited state is Coriolis coupled to the ground state, which then interacts with the 3B_1 state by spin-orbit coupling. The known thermochemistry is consistent with dissociation to Ge(3P)+H₂ occurring on the triplet state surface.

In contrast to the paucity of experimental data, there have been a substantial number of theoretical studies of GeH₂.^{20–32} Only the most relevant of these will be discussed. The ground state geometric parameters of GeH₂ have been predicted^{20,26,30} in the range $r(\text{Ge-H})=1.587\text{--}1.607$ Å and $\theta(\text{HGeH})=90.4\text{--}91.5^\circ$. By fitting 37 calculated points on the ground state potential energy surface, Bunker *et al.*³⁰ obtained the vibrational frequencies $\nu_1=1857$ cm⁻¹, $\nu_2=923$ cm⁻¹, and $\nu_3=1866$ cm⁻¹, in good agreement with the matrix data.¹⁵ The energy separation of the excited triplet and ground singlet states is predicted^{20,26,29} to be in the range of 22.8–23.6 kcal/mol (7974–8254 cm⁻¹), with an increase in the bond angle of 28.4–29.8° and a corresponding decrease in the bond length of 0.046–0.056 Å on excitation. The triplet state vibrational frequencies obtained from the calculated potential energy surface²⁹ were $\nu_1=1991$ cm⁻¹, $\nu_2=763$ cm⁻¹, and $\nu_3=2012$ cm⁻¹. The first excited singlet (1B_1) state was calculated by Balasubramanian²⁶ to be 47.3 kcal/mol (16 543 cm⁻¹) above the ground state with $r(\text{Ge-H})=1.553$ and $\theta(\text{HGeH})=122.1^\circ$, using relativistic CI methods. Barthelat *et al.*³¹ obtained $\Delta E(S_1-S_0)=46.7$ (16 334 cm⁻¹) with $r(\text{Ge-H})=1.566$ and $\theta(\text{HGeH})=123.2^\circ$ and vibrational frequencies of $\nu_1=1864$, $\nu_2=860$, and $\nu_3=2011$ cm⁻¹ for the S_1 state, using CI methods with core potentials.

In recent years, we have embarked on a program to study the jet-cooled electronic spectra of divalent group IVA reactive intermediates. We have succeeded in producing LIF spectra of CCl₂,³³ CClF,³⁴ CF₂,³⁵ SiCl₂,³⁶ SiF₂,³⁷ GeCl₂,³⁸ and GeF₂³⁹ with sufficient resolution to resolve the vibrational and, in favorable cases, the rotational structure in spectra that are often impossibly congested at room temperature. In the case of GeCl₂, GeF₂, and SiF₂, we have also been able to study the first excited triplet states through direct laser induced phosphorescence excitation spectroscopy. In the present work, we report the detection of jet-cooled GeH₂ by subjecting GeH₄ to an electric discharge at the exit of a pulsed valve. Several new bands have been found, the geometry of GeH₂ has been obtained from the rotational structure of the 0_0^0 band, fluorescence lifetimes have been measured for several excited state levels, and the germanium isotope effects have been measured. We have investigated the energetics of the excited state predissociation process with the aid of high quality *ab initio* calculations of the transition states and potential curves. Our more extensive results are in general agreement with previous work,^{16–18} although there are important differences.

II. EXPERIMENT

Germylene (GeH₂) was made using an electric discharge jet similar to many of the designs in the literature.^{40–45} In our apparatus, a mixture of 5% GeH₄ in argon (40–60 psi, Matheson) was expanded through the 0.8 mm orifice of a pulsed valve (General Valve, Series 9) into a 7 mm diameter flow channel drilled into a 14 mm long Teflon cylinder attached to the end of the valve. Halfway down the channel, two tungsten electrodes with pointed ends were mounted perpendicular to the gas flow with a 2 mm gap. At the appropriate time after triggering the valve, a 500 ns duration high voltage (2–6 kV) pulse was applied to one electrode, with the other electrode grounded. The resulting discharge efficiently dissociated germane, producing readily detectable quantities of GeH₂.

For measurements of the LIF spectrum of GeH₂, the pulsed free jet expansion was crossed with a tunable dye laser beam (Lambda-Physik FL 3002) 24 mm downstream from the end of the Teflon discharge block. The light emitted at right angles to the laser beam was imaged through appropriate cutoff filters onto the photocathode of a photomultiplier tube (EMI 9816QB) and the pulsed signals were processed with gated integrators. Low resolution spectra (0.1 cm⁻¹) were calibrated with optogalvanic lines of various neon- and argon-filled hollow cathode lamps. High resolution spectra (0.04 cm⁻¹), taken with an angle-tuned etalon in the laser cavity, were calibrated with laser induced fluorescence lines of iodine vapor. The GeH₂ laser induced fluorescence and calibration spectra were digitized and recorded simultaneously on a data acquisition system of our own design.⁴⁶

The pulsed discharge jet was mounted near the center of a large cylindrical (20 in. o.d.) vacuum chamber pumped by a 10 in. diffusion pump. The background chamber pressure was typically 2×10^{-6} Torr, rising to about 1×10^{-5} Torr when the pulsed valve (200–220 μ s gas pulses) was in operation. For the measurement of fluorescence lifetimes, considerable care was taken to guarantee that the data were collected sufficiently far downstream of the jet to ensure collision-free conditions. In a series of experiments, the distance of the excitation laser beam from the jet was augmented until the longest measured lifetimes (2.3 μ s) were invariant to further increases. All of the final measurements were done with the excitation laser beam 61 mm from the end of the Teflon discharge block, with optics that ensured that fluorescent molecules would not leave the detector viewing zone over at least two lifetimes. Fluorescence decays were recorded by digitizing the PMT output on a digital storage oscilloscope (LeCroy 9450A) with a temporal resolution of 2.5 ns per data point. The scattered laser light background was subtracted from the decay curve by slightly detuning the laser wavelength from the feature of interest. The decay curves were averaged over 500–1000 laser shots, background subtracted and transferred to a computer (IBM-PC) for analysis.

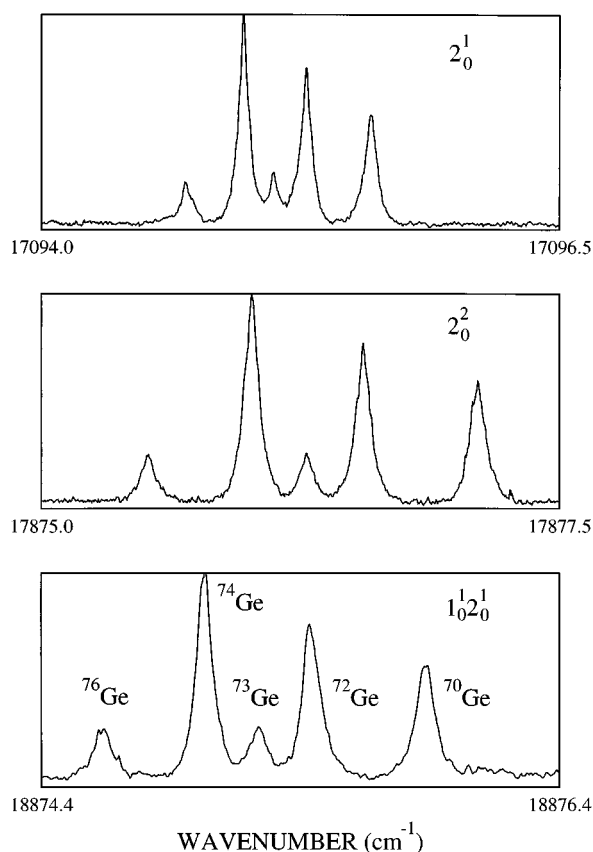


FIG. 1. Examples of high-resolution spectra of various vibronic bands of the $\tilde{A}^1B_1-\tilde{X}^1A_1$ system of GeH₂. In each case, the five features are due to the ${}^pP_1(1)$ transitions of the naturally abundant germanium isotopomers, as illustrated in the bottom spectrum.

III. EXPERIMENTAL RESULTS

A. Spectra

The lowest spin-allowed electronic transition of GeH₂ has been predicted to be the $\tilde{A}^1B_1-\tilde{X}^1A_1$ band system with onset near 610 nm,^{26,31} in excellent accord with the spectrum reported by Saito and Obi.¹⁶ *Ab initio* calculations^{26,31} suggest a bond angle increase of 30° and a bond length contraction of 0.034–0.041 Å on excitation, so that pronounced activity in both ν'_1 and ν'_2 would be expected in the spectrum, while the vibrational selection rules preclude activity in ν'_3 . GeH₂ is predicted to be a prolate asymmetric top in both the ground and excited states and the $\tilde{A}-\tilde{X}$ transition moment should be oriented out of the molecular plane, generating *C*-type vibronic bands obeying the selection rules $\Delta J=0, \pm 1$; $\Delta K_a=\pm 1$ and $\Delta K_c=0, \pm 2$. Germanium has five naturally occurring isotopes of significant abundance (⁷⁰Ge=20.5%, ⁷²Ge=27.4%, ⁷³Ge=7.8%, ⁷⁴Ge=36.5%, and ⁷⁶Ge=7.8%) so that each vibronic band is expected to show a multitude of isotopic splittings.

The discharge jet technique produced moderately strong LIF signals from GeH₂ in the 615–485 nm region, allowing us to positively identify ten vibronic bands, some examples of which are shown in Fig. 1. Saito and Obi^{16,18} were only able to observe the five 2_0^n ($n=0-4$) bands, presumably because the laser photolysis of phenylgermane produces

TABLE I. Vibrational assignments and estimated band origins of the observed vibronic bands of ⁷⁴GeH₂.

Assignment	Band origin ^a	Obs.–Calc. ^b
0 ₀ ⁰	16 325.544	–0.08
2 ₀ ¹	17 108.516	–0.04
2 ₀ ²	17 889.550	0.12
2 ₀ ³	18 668.381	0.11
2 ₀ ⁴	19 445.015	–0.07
2 ₀ ⁵	20 219.80	–0.06
1 ₀ ¹	18 123.977	0.26
1 ₀ 2 ₀ ¹	18 888.566	–0.27
1 ₀ 2 ₀ ²	19 651.671	–0.24
1 ₀ 2 ₀ ³	20 413.20	0.25

^aBand origin of the 0₀⁰ band from Table IV; other bands from ${}^pP_1(1)$ line +13.538 cm^{–1} (1_{1,0}–0_{0,0} interval in ground state). Origins quoted to three decimal places are ±0.01 cm^{–1}; others ±0.05 cm^{–1}.

^bCalculated using Eq. (1) and the parameters $T_0=16\,325.63(22)$, $\omega_1^{0'}$ = 1798.09(28), $\omega_2^{0'}=783.94(20)$, $x_{22}^{0'}=-1.018(38)$, $x_{12}^{0'}$ = –17.8(8); values in parentheses are standard errors of 1σ.

smaller quantities of the germylene. Each band was studied at high resolution but only the lowest energy vibronic band at 613 nm shows rotational structure; the other bands consist of a single line for each of the five naturally abundant isotopes of germanium, as illustrated in Fig. 1. These single lines are assigned as the ${}^pP_1(1)$ transition terminating on the lowest rotational level (0_{0,0} J_{K_a,K_c}) in each upper vibronic state, by analogy with SiH₂.^{16,19} The absence of any evidence of *r*-form branches originating in $K''_a=0$ is a strong indication of an inhomogeneous predissociation in the excited state.

Using the previous assignments of the bending progression¹⁶ and our *ab initio* estimate of $\nu'_1=1809$ cm^{–1} (*vide infra*), vibrational assignments were readily made for all the observed bands. The results are summarized in Table I. All of the bands are assigned as cold bands originating in the lowest vibrational level in the ground state, as expected for a molecule whose lowest vibrational frequency (ν''_2) is 917 cm^{–1}.¹⁶ The band origin for the ⁷⁴Ge isotopomer has been estimated in each case by adding the ground state 1_{1,0}–0_{0,0} interval (13.538 cm^{–1}) to the observed ${}^pP_1(1)$ transition frequency. To obtain the vibrational constants, the vibronic band origins were fitted to the anharmonic expansion

$$\bar{\nu}=T_{00}+\omega_1^{0'}\nu'_1+\omega_2^{0'}\nu'_2+x_{22}^{0'}\nu_2'^2+x_{12}^{0'}\nu_1'\nu_2'. \quad (1)$$

The results are reported in Table I, along with the observed–calculated values.

The lines of the different germanium isotopes were resolvable at high resolution for many of the higher vibronic bands. The wave numbers of the individual isotopic lines are given in Table II. As shown in Fig. 2, the germanium isotope shifts are linear with increasing quanta of the bending mode and extrapolate back to very small values for the 0₀⁰ band.

In contrast to Saito and Obi,¹⁶ who only observed three rotational lines in the 0₀⁰ band, we were able to observe a total of 18 lines, providing important information about the ground and excited states. The rotational structure of the band is shown in Fig. 3 and the measured transition frequencies and rotational assignments are summarized in Table III. Each rotational line in the band consists of contributions

TABLE II. Measured ${}^pP_1(1)$ isotopic line frequencies (cm⁻¹) for various vibronic bands of GeH₂.

	⁷⁶ GeH ₂	⁷⁴ GeH ₂	⁷³ GeH ₂	⁷² GeH ₂	⁷⁰ GeH ₂
2 ₀ ¹	17 094.693	17 094.978	17 095.122	17 095.280	17 095.589
2 ₀ ²	17 875.515	17 876.012	17 876.274	17 876.539	17 877.081
2 ₀ ³	18 654.131	18 654.843	18 655.205	18 655.601	18 656.398
2 ₀ ⁴	19 430.556	19 431.477	19 431.966	19 432.447	19 433.467
2 ₀ ⁵	...	20 206.26 ^a	...	20 207.44	20 208.68
1 ₀ ¹	18 110.295	18 110.439	...	18 110.612	18 110.801
1 ₀ ¹ ₀	18 874.641	18 875.028	18 875.238	18 875.437	18 875.883
1 ₀ ¹ ₂	19 637.521	19 638.133	19 638.460	19 638.781	19 639.464

^aThe lines of the 2₀⁵ band were outside the I₂ LIF range and were calibrated with optogalvanic lines to ±0.05 cm⁻¹.

from each of the five isotopomers of GeH₂, as the isotope shifts are unresolved at our laser resolution. It is noteworthy that we were able to observe a few very weak lines in the rR_0 and rQ_0 branches, terminating on upper state levels involving $K'_a = 1$. Two weak lines at 16 344.760 and 16 267.934 cm⁻¹ remain unassigned, although they may involve p -form transitions from $K''_a = 2$. The ground and excited state rotational constants were determined by a least-squares fitting of Watson's A reduction of the asymmetric top rotational Hamiltonian in the I' representation to the observed transition frequencies. In the fitting process, the ground and excited state rotational constants A , B , and C and the band origin, T_0 , were varied, yielding an overall standard deviation of fit of 0.008 cm⁻¹ for the 16 fitted transitions. The

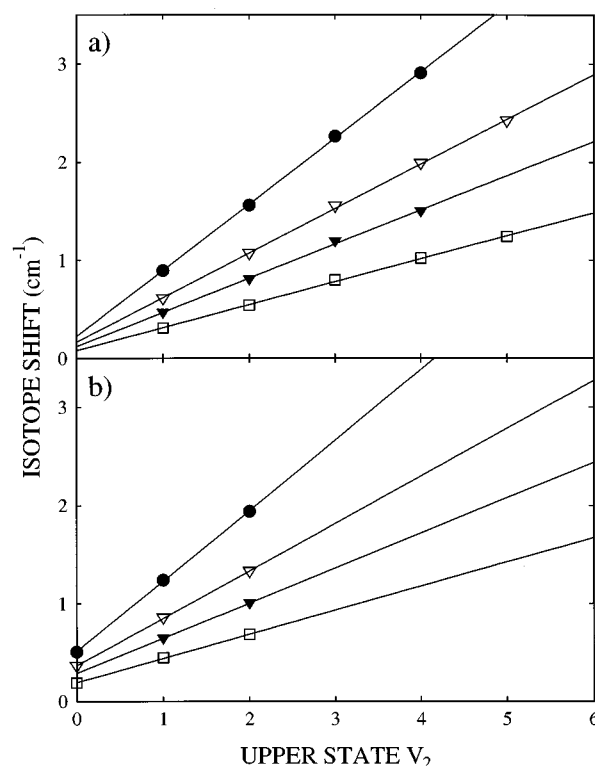


FIG. 2. Germanium isotope effects $[\bar{\nu}({}^{70}\text{GeH}_2) - \bar{\nu}({}^n\text{GeH}_2)]$ for the ${}^pP_1(1)$ lines of various vibronic bands of GeH₂. The isotope effects in (a) are for the 2₀ⁿ progression; those in (b) are for the 1₀¹2₀ⁿ progression. The symbol designations are: closed circle=⁷⁶GeH₂, open triangle=⁷⁴GeH₂, closed triangle=⁷³GeH₂, and open square=⁷²GeH₂.

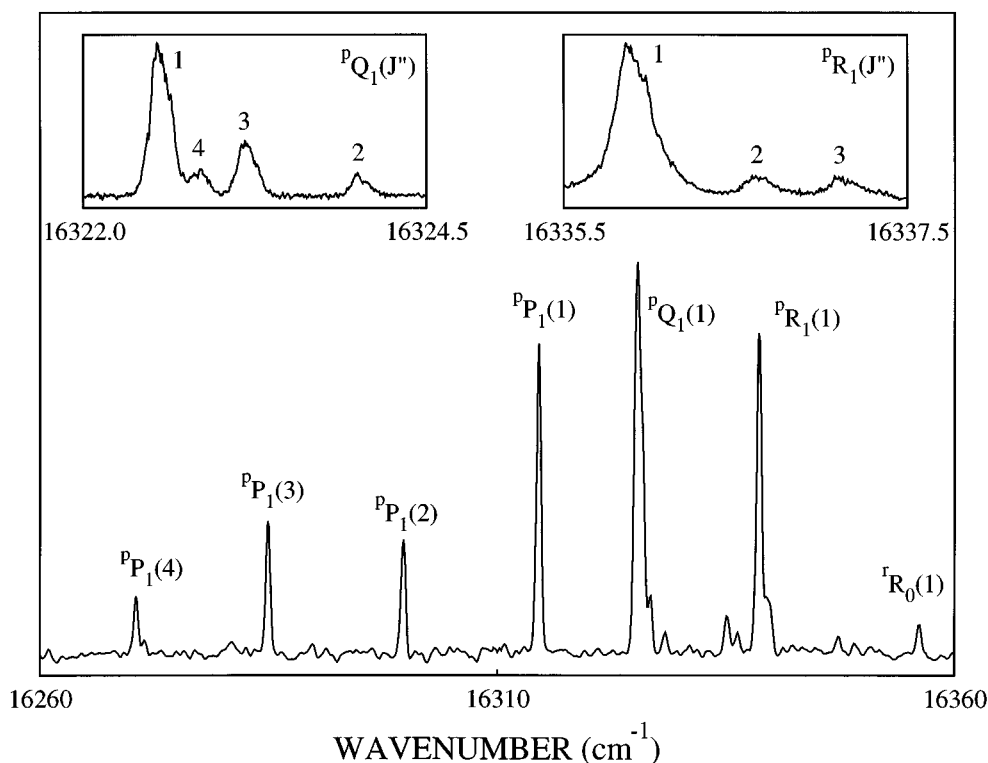


FIG. 3. The 0₀⁰ band of the $\tilde{A} \ ^1B_1 - \tilde{X} \ ^1A_1$ system of GeH₂. Rotational assignments of various lines are shown in the low-resolution spectrum at the bottom. The ${}^pP_1(4)$ assignment refers to the shoulder on the right-hand side of the lowest wavenumber feature in the spectrum. The insets show high-resolution spectra of portions of the band with the associated rotational assignments.

TABLE III. Rotational line frequencies (cm⁻¹) and assignments for the 0₀⁰ band of GeH₂.^a

Upper state			Lower state			Observed frequency	Obs.–Calc.
<i>J</i>	<i>K_a</i>	<i>K_c</i>	<i>J</i>	<i>K_a</i>	<i>K_c</i>		
4	1	3	3	0	3	16 372.604	-0.003
2	1	1	1	0	1	16 353.644	0.016
1	1	0	0	0	0	16 346.461	-0.016
4	0	4	3	1	2	16 337.119	-0.004
3	0	3	2	1	1	16 336.622	-0.003
2	0	2	1	1	0	16 335.895	0.012
2	1	2	2	0	2	16 333.504	-0.003
3	1	3	3	0	3	16 332.381	0.007
4	0	4	4	1	4	16 324.000	-0.007
1	0	1	1	1	1	16 323.189	-0.003
3	0	3	3	1	3	16 322.836	0.008
2	0	2	2	1	2	16 322.559	0.004
0	0	0	1	1	0	16 312.006	-0.009
1	0	1	2	1	1	16 297.064	-0.003
2	0	2	3	1	2	16 282.200	0.004
3	0	3	4	1	3	16 268.815	0.000

^aTwo additional unassigned lines were observed at 16 344.760 and 16 267.934 cm⁻¹.

fitted line frequencies and observed–calculated values are given in Table III and the resulting constants in Table IV.

The rotational constants obtained for the ground and excited states allow a determination of the effective (*r*₀) molecular structure in both states. Since only two moments are necessary to obtain a structure, three distinct calculations are possible, which should give the same structure if there is no inertial defect or experimental error in the constants. In general, one obtains slightly different structures even with very precise constants, due to the finite inertial defect. In the present case, we have calculated all the possible structures and report average values for the ground and excited states in Table IV.

B. Fluorescence lifetimes

We have measured fluorescence lifetimes of three rotational states in the 0⁰ vibronic level and for the 0_{0,0} rotational state for six higher vibronic states; the 2₀⁵, 1₀2₀², and 1₀2₀³

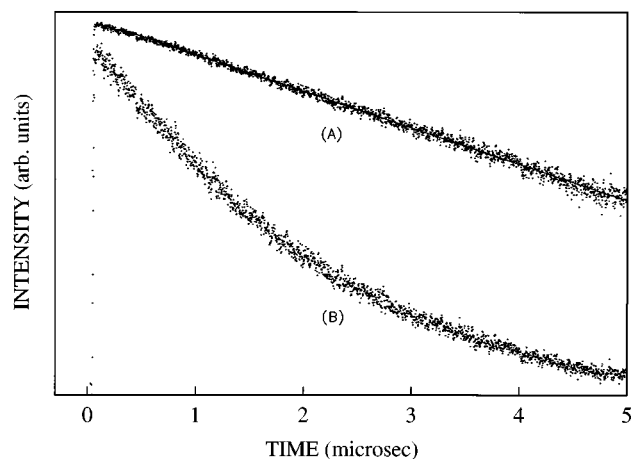


FIG. 4. Typical fluorescence decay data obtained on excitation of the 0₀⁰ band ^pP₁(1) transition. (A) Plot of the natural logarithm of the fluorescence intensity vs time. The least squares fitted line gave a lifetime of 2.28 μs over 2.2 lifetimes. (B) The same data with the ordinate plotted on a linear scale.

bands were too weak for reliable fluorescence lifetime measurements. In all cases, good single exponential decays were obtained over 2–3 lifetimes, with no evidence of geometric or collisional effects influencing the measurements. A typical decay curve following excitation of the ^pP₁(1) line of the 0₀⁰ band is illustrated in Fig. 4. The measured fluorescence lifetimes are reported in Table V. For the higher vibronic bands, no significant variations in fluorescence lifetimes could be found on excitation of the different GeH₂ isotopomers.

While our fluorescence lifetime measurements were in progress, Saito and Obi¹⁸ reported similar results for the bending levels of GeH₂ and GeD₂. Table V shows that the present results are in excellent accord with their data for the rotational levels of the lowest vibronic level but show substantial differences for higher vibronic levels, with our lifetimes being longer in all cases. The source of the discrepancy is difficult to ascertain. We have repeated our measurements under a variety of experimental conditions with consistent results. We also measured fluorescence lifetimes of SiH₂, prepared in the discharge jet by substituting SiH₄ for GeH₄. For the 2² (0_{0,0}) and 2⁶ (0_{0,0}) levels we obtained lifetimes of

TABLE IV. Comparison of experimental and *ab initio* molecular constants and geometric parameters of ⁷⁴GeH₂.

	Experiment		Theory		
	\tilde{X}^1A_1	\tilde{A}^1B_1	\tilde{X}^1A_1	\tilde{a}^3B_1	\tilde{A}^1B_1
<i>A</i>	6.9978(145) ^a	16.415 (21) ^a	6.9582 ^b	14.3103 ^c	15.2037 ^d
<i>B</i>	6.5314(84)	4.5182(30)	6.4504	4.6810	4.5288
<i>C</i>	3.3318(32)	3.4601(36)	3.3474	3.5272	3.4894
<i>T</i> ₀	0	16 325.544(18)	0	7975	16 543
<i>r</i> (Ge–H)(Å)	1.591(7)	1.553(12)	1.591	1.545	1.553
θ (H–Ge–H)(°)	91.2(8)	123.4(19)	91.4	119.8	122.1

^aValues in parentheses are 3σ values. The geometric parameters are averages over the three possible structures (see text) and the values in parentheses are the maximum deviation from the average.

^bReference 30.

^cReference 29.

^dReference 26.

TABLE V. Fluorescence lifetimes (in μs) of single rovibronic levels of GeH₂.

Vibronic level	Rotational level ($J_{K_aK_c}$)	This work	Ref. 18
0^0	0_{00}	2.28 ± 0.02	2.29 ± 0.07
	1_{01}	0.967 ± 0.010	0.97 ± 0.01
	2_{02}	0.136 ± 0.005	0.13 ± 0.03
2^1	0_{00}	1.79 ± 0.02	1.30 ± 0.26
2^2	0_{00}	1.45 ± 0.02	0.81 ± 0.01
2^3	0_{00}	1.26 ± 0.02	0.72 ± 0.04
2^4	0_{00}	1.06 ± 0.02	0.64 ± 0.05
1^1	0_{00}	2.32 ± 0.02	...
1^2_1	0_{00}	1.94 ± 0.02	...

1.07 ± 0.01 and 0.79 ± 0.01 μs , respectively, comparable to literature values¹⁹ of 1.0 ± 0.27 and 0.60 ± 0.03 μs . An examination of the published decay curve for the GeH₂ 2^2 level¹⁸ shows noticeable deviations from single exponential behavior at longer times (beyond 2 μs), indicative of geometric effects due to excited state molecules leaving the detector viewing zone. The experimental parameters¹⁸ (800 μm orifice, 1 atm argon, excitation 19 nozzle diameters downstream of the jet and 12.5 diam after photolysis, chamber pressure 10^{-4} Torr) also appear insufficient to ensure collision-free conditions. In our work, we found that the fluorescence lifetimes were quite sensitive to the experimental conditions, particularly the distance downstream of the jet, as expected if collisional quenching is important. If all of our lifetimes, including those of the 0^0 level, were longer than those of Saito and Obi, the discrepancy could probably be satisfactorily explained as due to collisional or geometric effects. The fact that the longest lifetimes are in agreement is more difficult to rationalize, although the effect may be due to more efficient collisional quenching of the higher vibrational levels.

The present lifetime measurements are in much better agreement with expectations from theory than were previous results. In published work on SiH₂, it was shown¹⁹ that plots of the 2^n ($n=0-6$; $0_{0,0}$ rotational state) level fluorescence decay rates vs the cube of the transition energy times the sum of the Franck–Condon factors yielded a straight line with near-zero intercept. These results imply that the lowest rotational levels decay purely radiatively, as expected for a predissociation process that involves Coriolis coupling to the ground state. Similar results would be expected for GeH₂, but Saito and Obi¹⁸ found that their plot gave a straight line with a substantially negative intercept. In Fig. 5, we have replotted the SiH₂ and GeH₂ data including the present results. We have neglected the Franck–Condon factor summation, as the sum is found to be nearly constant for the present range of upper state vibronic levels^{18,19} and the Franck–Condon factors can only be approximated without more complete information on the ground and excited state vibrational force fields.⁴⁷ We find that our lifetime data gives a good linear plot with an intercept closer to zero than previous SiH₂ data, whereas the literature lifetimes for GeH₂ have considerably more scatter and deviate much further from a

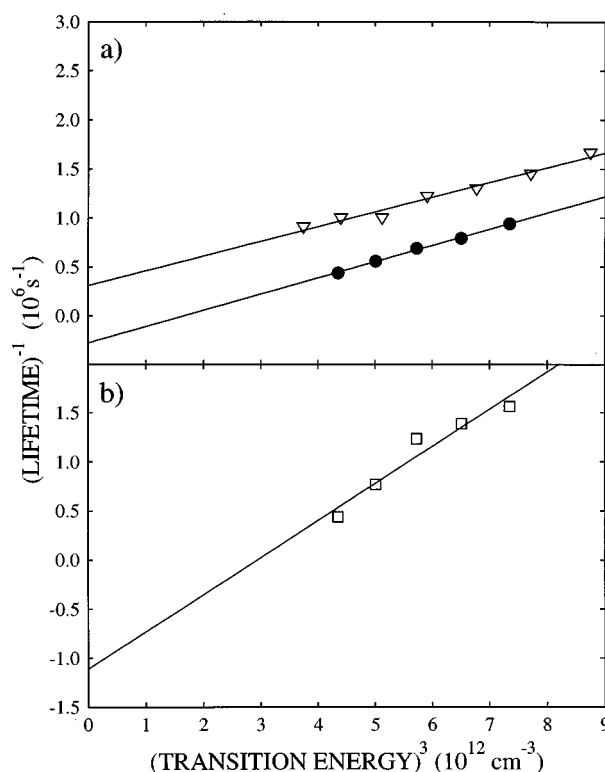


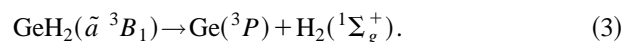
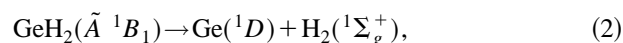
FIG. 5. Plots of the inverse lifetime of the $0_{0,0}$ rotational levels of the 2^n vibronic levels of the \tilde{A} states of SiH₂ and GeH₂ vs the third power of the transition energy of the vibronic band. In (a), the results for SiH₂ (open triangles, Ref. 19) and GeH₂ (closed circles, present work) are compared. In (b), previous data for GeH₂ (open squares, Ref. 18) are presented.

zero intercept, suggesting that the current results are more reliable.

IV. THEORETICAL STUDIES

A. Methods

The goal of these theoretical studies was to characterize those features of the excited state potential energy surfaces responsible for the excited state dissociation processes. Thus, we used the full-valence complete-active-space self-consistent-field method (CASSCF), because it can describe regions of the potential energy surface where bond breaking and spin recoupling are important.⁴⁸ The equilibrium geometries of the \tilde{X}^1A_1 , \tilde{a}^3B_1 , and \tilde{A}^1B_1 electronic states were precisely determined at the CASSCF level of theory using analytical gradient techniques, as were the transition states corresponding to the reactions



All stationary points were characterized as minima or transition states by determining the nuclear Hessian, and associated harmonic vibrational frequencies, via central finite difference methods.

Polarized triple-zeta quality basis sets were used for the geometry optimization. Specifically, for hydrogen we employed Dunning's (5s/3s) contraction of Huzinaga's primi-

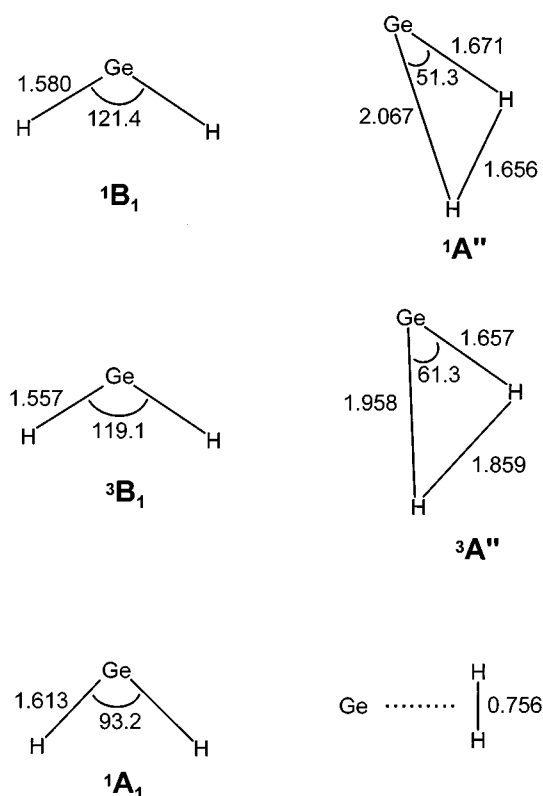


FIG. 6. Stationary points on the GeH₂ potential energy surfaces at the complete-active-space self-consistent-field level of theory using a polarized triple zeta basis set, TZ(2*df*,2*p*). The structures on the left are the reactants and their corresponding transition states (or products) are shown on the right.

tive set,⁴⁹ with two sets of *p* functions added [$\alpha_p(H)=1.5$ and 0.375]. The germanium basis set was derived from Dunning's 14*s*11*p*5*d* primitive set,⁵⁰ initially contracted to 8*s*6*p*3*d* in a (61121111/611111/311) fashion. Subsequently, the two valence *s* and *p* functions were replaced by a set of three functions with exponents $\alpha_s(\text{Ge})=0.376$, 0.151, 0.06, and $\alpha_p(\text{Ge})=0.382$, 0.153, 0.061 corresponding to 2.5 μ , μ , and $\mu/2.5$ where μ is the corresponding geometric mean of the original two *s* and *p* functions. Finally, additional sets of *d*-functions ($\alpha_d=0.25$, 0.08) and a single *f* function ($\alpha_f=0.34$) were appended to the germanium basis set. Using pure spherical harmonic *d* and *f* gaussians, the resulting basis set—technically designated Ge(15*s*12*p*7*d*1*f*/

9*s*7*p*5*d*1*f*) and H(5*s*2*p*/3*s*2*p*)—contains 80 functions. We will refer to this basis set as TZ(2*df*,2*p*).

Our final energy predictions used larger atomic natural orbital (ANO) basis sets⁵¹ and second-order configuration interaction (SOC) energies at the CASSCF TZ(2*df*,2*p*) optimized geometries. The hydrogen ANO set is the density matrix averaged (8*s*4*p*3*d*)/[3*s*2*p*1*d*] generalized contraction of Widmark *et al.*,⁵² while the germanium ANO set is of the form (20*s*15*p*11*d*3*f*1*g*)/[7*s*6*p*4*d*2*f*1*g*]. The latter was constructed from the valence CISD natural orbitals obtained with Partridge's 20*s*15*p*9*d* primitive gaussian basis set,⁵³ and the following appended polarization functions: $\alpha_d=0.1431$, 0.05724; $\alpha_f=0.85$, 0.34, 0.136; $\alpha_g=0.48$. The SOC is a single and double excitation multireference CI method in which all configurations of the CASSCF act as references; it is known to yield energies in excellent agreement with full CI for chemical systems where the full CI can be obtained.⁵⁴

B. Results

The CASSCF/TZ(2*df*,2*p*) optimized geometries of the three electronic states of GeH₂ and the transition states and products for reactions (2) and (3) are shown in Fig. 6. Because the CASSCF method mainly includes near-degeneracy electron correlation effects, but lacks significant dynamical correlation, bond distances are usually too long at this level of theory.⁴⁸ GeH₂ appears to be normal in this respect: the bond distances are longer than experimental values for the ground and excited singlet state by 0.02–0.03 Å. For similar reasons, CASSCF harmonic vibrational frequencies are often in fortuitously good agreement with experimentally observed fundamental frequencies, as is found in the present case (see Table VI).

The transition state geometries for dissociation of the \tilde{a} ³B₁ and \tilde{A} ¹B₁ states (reactions 2 and 3) have C_s symmetry, resulting in ³A'' and ¹A'' states (see Fig. 6). The lowered symmetry results from an avoided crossing with electronic states of A₂ symmetry, as discussed previously for SiH₂.^{55,56} These transition state geometries are intermediate between those of the reactants and products; for example, one of the Ge–H distances is 0.4–0.5 Å longer than in GeH₂, but the H–H distance is still far from the equilibrium distance in H₂. Transition state geometries midway between reactants and products are expected for an approximately thermoneutral

TABLE VI. Experimentally determined and theoretically predicted vibrational frequencies (cm⁻¹) for GeH₂.

	Experiment ^a				Theory			
	ν_1	ν_2	ν_3	Reference	ν_1	ν_2	ν_3	Reference
\tilde{X} ¹ A ₁	1887	920	1864	15	1857	923	1866	30 ^b
	1840	913	1840	this work
\tilde{a} ³ B ₁	1991	763	2012	29 ^b
	1998	801	2054	this work
\tilde{A} ¹ A ₁	...	~780	...	18	1864	860	2011	31
	1798	783	...	this work	1809	783	1909	this work

^aFundamental vibrational frequencies.

^bFundamental vibrational frequencies from a fitted potential surface.

TABLE VII. Relative energies (kcal/mol) of the various optimized geometries of GeH₂ at the complete-active-space self-consistent-field (CASSCF) and second-order configuration interaction (SOC) level of theory using basis sets of polarized triple zeta (TZ(2*df*,2*p*)) and [7*s*6*p*4*d*2*f*1*g*/3*s*2*p*1*d*] atomic natural orbital (ANO) form.

Electronic state	CASSCF		SOC	
	TZ(2 <i>df</i> ,2 <i>p</i>)	ANO	TZ(2 <i>df</i> ,2 <i>p</i>)	ANO
GeH ₂ (\tilde{A}^1B_1)	46.3	46.2	46.1	45.7
GeH ₂ ($^1A''$ transition state)	72.0	72.0	69.0	69.4
Ge(1D)+H ₂ ($^1\Sigma_g^+$)	50.3	49.8	48.9	49.5
GeH ₂ (\tilde{a}^3B_1)	21.4	21.7	22.7	23.0
GeH ₂ ($^3A''$ transition state)	66.7	66.9	64.2	64.9
Ge(3P)+H ₂ ($^1\Sigma_g^+$)	28.0	28.0	29.9	31.6
GeH ₂ (\tilde{X}^1A_1) ^a	0.0	0.0	0.0	0.0

^aThe absolute energies of the ground \tilde{X}^1A_1 electronic state are: CASSCF/TZ(2*df*,2*p*) -2076.410 223; CASSCF/ANO -2076.568 711; SOC/TZ(2*df*,2*p*) -2076.487 485; SOC/ANO -2076.651 699.

reaction, which is the case here. The three harmonic vibrational frequencies associated with the $^1A''$ state are 1540, 677, and 785i cm⁻¹, while those for $^3A''$ are 1633, 78, and 1628i cm⁻¹; the single imaginary frequency in each case verifies that these are transition states. The larger magnitude imaginary frequency associated with the triplet state reaction correlates with the larger barrier height found for that case (*vide infra*).

The relative energies are shown in Table VII. Note that increasing both the quality of the basis set and the correlation method leads to only small (<4 kcal/mol) changes in the relative energies compared to our base CASSCF/

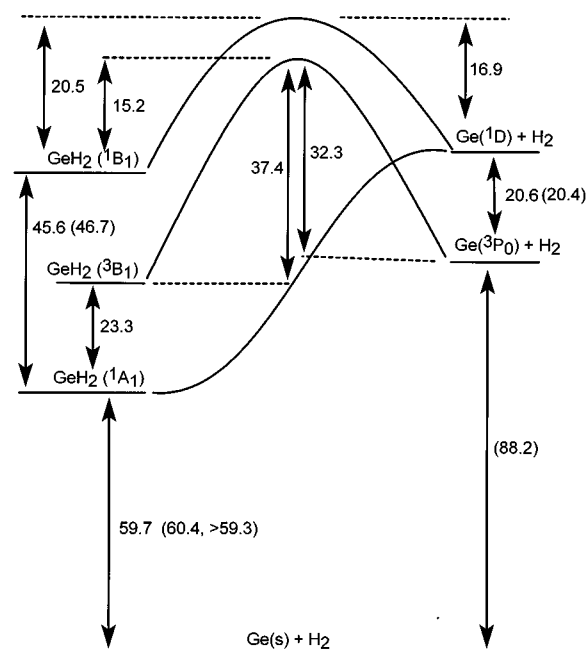


FIG. 7. A schematic potential energy profile for the three electronic states of GeH₂ and their asymptotes, relative to the standard state of solid germanium, Ge(s), and molecular hydrogen. Relative energies (kcal/mol) are determined at the second-order configuration interaction (SOC) level of theory using atomic natural orbital (ANO) basis sets, and have been corrected for zero-point energies and atomic spin-orbit splitting.

TZ(2*df*,2*p*) results. In terms of quantities that can be directly compared to experiment, the largest effect of these theoretical enhancements is for the Ge(3P)-Ge(1D) energy difference, which changes from 7808 cm⁻¹ (22.3 kcal/mol) at the CASSCF/TZ(2*df*,2*p*) level of theory to 6251 cm⁻¹ (17.9 kcal/mol) at the SOC/ANO level of theory. To directly compare these values to spectroscopically determined atomic state energy differences, we need to apply spin-orbit corrections, because the quantities we obtain from our theoretical studies correspond to term averages; i.e., averages over all the *J* states for a given term. Thus, the term average energy, E_{av} , obtained theoretically should be corrected by

$$E_{av}(^3P) - E(^3P_0) = [E(^3P_0) + 3E(^3P_1) + 5E(^3P_2)]/9 - E(^3P_0) \quad (4)$$

or 969 cm⁻¹ from spectroscopy.⁵⁷ The final result is a spin-orbit corrected prediction for $E(^1D_2) - E(^3P_0)$ of 7220 cm⁻¹ (20.6 kcal/mol) at the SOC/ANO level of theory, in excellent agreement with the experimental value of 7125 cm⁻¹ (20.4 kcal/mol).⁵⁷

To compare most energy differences with experimental quantities we must correct for zero-point vibrational energy differences. Here we have approximated⁵⁸ the zero-point energies as one-half the sum of the predicted harmonic vibrational frequencies, except for H₂, where the exact value of 6.21 kcal/mol is used.⁵⁸ After making these corrections, we obtain the schematic potential energy surface in Fig. 7. Note that the triplet germanium atom enthalpy includes the spin-orbit correction discussed above, but that no correction has been made to the other triplet state energies. For GeH₂(3B_1), this is justified from previous relativistic CI calculations that showed the three spin-orbit components of this state differed by only 0.12 kcal/mol.²⁶ For the transition state, it is still probably reasonable to assume that spin-orbit effects are small.

In those cases where we can compare our theoretically predicted enthalpies to experiment, the agreement is excellent. For example, the $\tilde{A}^1B_1 - \tilde{X}^1A_1$ enthalpy difference is predicted to be 45.6 kcal/mol, compared to the experimental result of 46.7 kcal/mol. Also, from the GeH₂(\tilde{X}^1A_1) → Ge(3P_0) + H₂($^1\Sigma_g^+$) enthalpy difference, and the experimental value for the heat of formation of the germanium atom (0 K) of 88.2 ± 0.7 kcal/mol recommended by Berkowitz,⁵⁹ we predict $\Delta H_f^0(\text{GeH}_2) = 59.7$ kcal/mol, compared to experimental values of 60.4 ± 3.8 (Ref. 60) and >59.3 (most probably 61.8) kcal/mol.⁵⁹ In conclusion, the theoretical predictions for the atomic germanium states, the GeH₂ singlet states and the heat of formation of GeH₂, which connects the atomic and molecular states, all agree with experiment to within about 1 kcal/mol. This gives us confidence in those theoretical predictions which cannot be directly compared with experiment.

V. DISCUSSION

In this work, we have been able to determine the ground and excited state molecular structures of GeH₂ for the first time. Previous *ab initio* predictions of the equilibrium geometric parameters (Table IV) are in good agreement with the

present r_0 values. It is fortunate that the discharge jet technique provided strong enough LIF signals and sufficiently high rotational temperatures to allow us to record a more extensive range of transitions than in previous work.¹⁶

The present *ab initio* predictions of the excited state harmonic vibrational frequencies are in excellent accord with the experimentally observed fundamentals (Table VI). For the ground state, our theoretical predictions are in agreement with previous more detailed calculations,³⁰ which involved fitting points on the ground state potential energy surface. There is still some uncertainty as to whether ν_1 or ν_3 is larger, as theory and experiment give conflicting results. However, the matrix spectrum¹⁵ was assigned with $\nu_1 > \nu_3$ solely on the basis of an observed splitting in one of the fundamentals of GeD₂, attributed to Fermi resonance between ν_1 and $2\nu_2$, and there is some question about the validity of this conclusion.

As a check on the vibrational analysis of the electronic spectrum, we have calculated the expected isotope shifts for the 0_0^0 band of the $\tilde{A}-\tilde{X}$ transition, from the ground and excited state *ab initio* harmonic frequencies. For ⁷⁴GeH₂/⁷⁴GeD₂, we predict a 14.3 cm⁻¹ shift on deuteration, in good agreement with the 11 ± 2 cm⁻¹ shift measured by Saito and Obi.¹⁶ Similarly, we predict small (<0.2 cm⁻¹) shifts for the various germanium isotopomers, in agreement with those observed (see Fig. 2). If the vibrational numbering of the 2_0^n progression were shifted by one unit in either direction, the discrepancy between the observed and calculated isotope shifts would be unacceptably large. Similarly, the inertial defect for the 0^0 level of GeH₂ (0.1140 amu Å²) is comparable to that of SiD₂ (Ref. 61) (0.138 amu Å²); if our 0_0^0 band were actually 2_0^1 the upper state inertial defect would be expected to be substantially larger (SiD₂ $2_0^1 = 0.4067$ amu Å²). The isotope shift and inertial defect data leave little doubt that the vibrational analysis is correct.

Much of the spectroscopy and excited state decay dynamics of GeH₂ can be understood in the context of our more extensive knowledge of SiH₂, which we briefly summarize here. Silylene absorbs in the 650–480 nm region,⁶² much of the rotational structure is perturbed and the fluorescence lifetimes of single rovibronic levels vary widely.⁶³ At low excited state vibrational energies, SiH₂ predissociates to Si(³P)+H₂(¹Σ_g⁺), as shown by photofragment excitation spectroscopic detection of Si(³P).⁶⁴ Jet spectroscopy of SiH₂ reveals that only the few lowest rotational levels in the lower vibronic states of SiH₂ fluoresce and that the fluorescence lifetimes decrease with increasing rotational angular momentum.¹⁹ More extensive rotational structure is found in the LIF spectra of jet-cooled SiD₂, but most of the structure disappears at higher vibrational energies.⁶¹ Fukushima *et al.*¹⁹ concluded that all these observations were consistent with a rotationally dependent predissociation process involving second-order coupling of the type $\tilde{A}^1B_1 - (\text{Coriolis}) \rightarrow \tilde{X}^1A_1 - (\text{spin-orbit}) \rightarrow \tilde{a}^3B_1$ state. Energetic and spin conservation rules dictate that the predissociation should occur from the triplet manifold and the \tilde{A}^1B_1 state cannot interact directly with the \tilde{a}^3B_1 state through spin-orbit coupling.⁶⁵ Coriolis coupling between the \tilde{A} and \tilde{X} states would not occur for the $0_{0,0}$ rotational level, explain-

ing the observation that fluorescence from this level persists even at higher excited state vibrational energies. The differences in the jet spectra of SiH₂ and SiD₂ have been interpreted¹⁹ as due to a potential barrier in the dissociation of \tilde{a}^3B_1 to Si(³P)+H₂, in qualitative agreement with *ab initio* studies⁵⁶ of the energetics and transition states involved in the dissociation of SiH₂.

At high vibrational energies in the excited states of SiH₂ and SiD₂, the abrupt onset of the Si(¹D)+H₂(¹Σ_g⁺) dissociation channel appears, as indicated by Si(¹D) photofragment⁶⁶ and fluorescence lifetime studies.^{56,19} *Ab initio* studies⁵⁶ suggest that there is no reverse barrier to this process, so that dissociation occurs once the \tilde{A} state energy equals that of the products. However, lifetime studies¹⁹ of SiH₂ and SiD₂ show a distinct isotope effect for this process, suggesting the existence of a potential barrier and a tunneling predissociation mechanism.

All of the available experimental data support the view that GeH₂ undergoes predissociation processes from the \tilde{A}^1B_1 state, similar to those in SiH₂, as originally proposed by Saito and Obi.¹⁶ The $v_2' = 0$ level of GeH₂ and the $v_2' = 0, 1,$ and 2 levels of GeD₂ only show fluorescence from low angular momentum rotational states, indicative of a J -dependent predissociation process. The measured fluorescence lifetimes of various rotational states of the GeH₂ 0^0 level (Table V) decrease by more than an order of magnitude from $J=0$ to $J=2$, clearly showing the J dependence. For higher vibrational levels, only transitions to the $0_{0,0}$ rotational level are observed by LIF; the excited state rotational levels with nonzero rotational angular momentum do not give rise to detectable fluorescence. The smooth variation of the measured fluorescence lifetimes for the $0_{0,0}$ rotational levels with excited state vibrational energy (Fig. 5) indicates that the decay is purely radiative, without a substantial non-radiative component. Thus, without the enabling effect of molecular rotation, the lower vibrational levels of \tilde{A}^1B_1 GeH₂ decay radiatively, whereas levels with rotational angular momentum decay nonradiatively.

Saito and Obi¹⁸ found a breaking off in the LIF spectra at $v_2' = 4$ (3120 cm⁻¹ of vibrational energy) for GeH₂ and $v_2' = 6$ (3337 cm⁻¹ of vibrational energy) for GeD₂. With the increased sensitivity of our experiment, we were able to observe the $v_2' = 5$ level and $\nu_1' + \nu_2'$ combination levels up to 4088 cm⁻¹ of vibrational energy in GeH₂. Calculated Franck-Condon factors¹⁸ show that the absorption spectra extend well beyond the breaking off of the LIF spectra, implying that a second nonradiative channel involving even the $0_{0,0}$ levels appears at high vibrational energies.

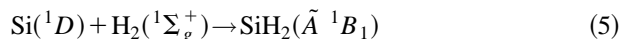
Referring to Fig. 7, the present experimental results on GeH₂ and previous work¹⁶⁻¹⁸ on GeD₂ can be rationalized by a model similar to that used for SiH₂. Employing the best available thermodynamic and spectroscopic data, (experimental data in Fig. 7), we calculate that the Ge(¹D)+H₂ products are 0.5–2.5 kcal/mol above the $S_1 v=0$ level, so that predissociation of this level yields Ge(³P)+H₂. The lower vibrational levels of GeH₂ and GeD₂ show J -dependent and isotope-dependent nonradiative decay processes which can be ascribed to second-order coupling from S_1 through S_0 to T_1 . Although the energy of the Ge(³P)+H₂

products is below the S_1 state, our *ab initio* results show a barrier to the dissociation, suggesting that tunneling through the barrier must occur, consistent with the observed differences in dynamics between GeH₂ and GeD₂.

For higher vibrational levels of GeH₂ and GeD₂, there are two possible processes: coupling through S_0 to T_1 and tunneling through the barrier to yield Ge(³P), or direct tunneling through the potential barrier from S_1 to form Ge(¹D)+H₂. In the former case, the $0_{0,0}$ levels, which cannot Coriolis couple to S_0 , would be expected to decay radiatively, as observed. In the latter case, the fluorescence lifetimes of the $0_{0,0}$ levels would be expected to decrease substantially at vibrational energies above the enthalpy of the Ge(¹D)+H₂ products, which should occur between $v_2' = 0$ and 2 for both GeH₂ and GeD₂. The fact that there are no anomalies in the rotational structure or fluorescence lifetimes of the 2_0^1 or 2_0^2 bands of either isotopomer leads us to conclude that dissociation to form Ge(¹D) is not the predominant decay process for any of the levels observed in the LIF experiments.

The breaking off of fluorescence from higher vibronic levels of germylene suggests that the second dissociation process to form Ge(¹D) becomes important at about 4000 cm⁻¹ or 11.4 kcal/mol of vibrational energy in the S_1 state. As the barrier to this dissociation is calculated to be 20.5 kcal/mol above the S_1 state, tunneling through the barrier must occur. If sufficiently sensitive LIF experiments could be done, we would anticipate that GeD₂ levels above those of GeH₂ would be detected and that the $0_{0,0}$ level lifetimes of both isotopomers would decrease substantially in the region where the second dissociation process becomes significant. To clarify the role of the two dissociation processes, we are currently designing an experiment to observe the Ge(³P) and Ge(¹D) products spectroscopically following state-selected photodissociation of \tilde{A}^1B_1 germylene.

An important feature of the excited singlet surface of GeH₂ is the existence of a substantial barrier to the reaction forming Ge(¹D) in excess of the endothermicity, as shown in Fig. 7. This is in contrast to published discussions of SiH₂ excited state dynamics,^{56,66} where it was believed that the reaction



was essentially barrierless. Apparently, this belief arose from a theoretical study⁵⁶ of this reaction, but close scrutiny of the calculations shows a major deficiency: they disagree with experimental facts for the dissociation channel energetics of Si(¹D)+H₂ vs Si(³P)+H₂, which involves the Si(¹D)–Si(³P) energy difference. Theory predicts 29.9 kcal/mol for the atomic state splitting,⁵⁶ whereas the accurate experimental value is 18.0 kcal/mol. Clearly, the unrestricted Hartree–Fock, spin-projected MP studies are not accurate for this region of the potential energy surface, and the conclusion that Si(¹D) insertion into H₂ is a barrierless process is suspect. More recent experimental work by Fukushima *et al.*¹⁹ supports this view, because SiD₂ and SiH₂ show different decay dynamics at comparable vibrational energies in the region of the onset of the dissociation channel that produces Si(¹D). The existence of a barrier to the dissociation

process in the excited state also implies that it is inaccurate to use the breaking off of fluorescence¹⁸ or the onset of the second reaction channel¹⁹ as the dissociation limit in calculating the heats of formation of SiH₂ or GeH₂.

ACKNOWLEDGMENTS

The authors thank Chris Chan of the University of British Columbia for providing us with his design for a pulsed discharge circuit and Yukio Yamaguchi for the CASSCF program used in this work. We acknowledge the University of Kentucky Center for Computational Sciences and the Computer Center of the University of Kentucky for aid in the theoretical calculations. This research was supported by the National Science Foundation.

- ¹W. Du, L. A. Keeling, and C. M. Greenleaf, *J. Vac. Sci. Technol. A* **12**, 2281 (1994).
- ²C. Isobe, H. Cho, and J. E. Crowell, *Surf. Sci.* **295**, 117 (1993).
- ³V. Tavitian, C. J. Kiely, D. B. Geohegan, and J. G. Eden, *Appl. Phys. Lett.* **52**, 1710 (1988).
- ⁴J. F. Osmundsen, C. C. Abele, and J. G. Eden, *J. Appl. Phys.* **57**, 2921 (1985).
- ⁵J. M. Baribeau, T. E. Jackman, D. C. Houghton, P. Maigne, and M. W. Denhoff, *J. Appl. Phys.* **63**, 5738 (1988).
- ⁶Y. Kataoka, H. Ueba, and C. Tatsuyama, *J. Appl. Phys.* **63**, 749 (1988).
- ⁷G. Lucovsky, *J. Non-Cryst. Solids* **76**, 173 (1985).
- ⁸A. H. Mahan, D. L. Williamson, and A. Madan, *Appl. Phys. Lett.* **44**, 220 (1984).
- ⁹W. Paul, S. J. Jones, W. A. Turner, and P. Wickboldt, *J. Non-Cryst. Solids* **141**, 271 (1992).
- ¹⁰G. Lu and J. E. Crowell, *J. Chem. Phys.* **98**, 3415 (1993).
- ¹¹C. G. Newman, J. Dzarnoski, M. A. Ring, and H. E. O'Neal, *Int. J. Chem. Kinet.* **12**, 661 (1980).
- ¹²T. Motooka and J. E. Greene, *J. Appl. Phys.* **59**, 2015 (1986).
- ¹³A. Lloret, M. Oria, B. Seoudi, and L. Abouaf-Marguin, *Chem. Phys. Lett.* **179**, 329 (1991).
- ¹⁴J. E. Crowell and G. Lu, *J. Electron Spectrosc. Related Phenom.* **54**, 1045 (1990).
- ¹⁵G. R. Smith and W. A. Guillory, *J. Chem. Phys.* **56**, 1423 (1972).
- ¹⁶K. Saito and K. Obi, *Chem. Phys. Lett.* **215**, 193 (1993).
- ¹⁷K. Obi, M. Fukushima, and K. Saito, *Appl. Surf. Sci.* **79**, 465 (1994).
- ¹⁸K. Saito and K. Obi, *Chem. Phys.* **187**, 381 (1994).
- ¹⁹M. Fukushima, S. Mayama, and K. Obi, *J. Chem. Phys.* **96**, 44 (1991).
- ²⁰C. J. Cramer, F. J. Dulles, J. W. Storer, and S. E. Worthington, *Chem. Phys. Lett.* **218**, 387 (1994).
- ²¹K. G. Dyall, *J. Chem. Phys.* **96**, 1210 (1992).
- ²²K. K. Das and K. Balasubramanian, *J. Chem. Phys.* **93**, 5883 (1990).
- ²³R. C. Binning, Jr. and L. A. Curtiss, *J. Chem. Phys.* **92**, 3688 (1990).
- ²⁴R. C. Binning, Jr. and L. A. Curtiss, *J. Chem. Phys.* **92**, 1860 (1990).
- ²⁵M. C. Kerins, N. J. Fitzpatrick, and M. T. Nguyen, *Theochem* **49**, 297 (1988).
- ²⁶K. Balasubramanian, *J. Chem. Phys.* **89**, 5731 (1988).
- ²⁷A. Selmani and D. R. Salahub, *J. Chem. Phys.* **89**, 1529 (1988).
- ²⁸L. G. M. Pettersson and P. E. M. Siegbahn, *Chem. Phys.* **105**, 355 (1986).
- ²⁹R. A. Phillips, R. J. Buenker, R. Beardsworth, P. R. Bunker, P. Jensen, and W. P. Kraemer, *Chem. Phys. Lett.* **118**, 60 (1985).
- ³⁰P. R. Bunker, R. A. Phillips, and R. J. Buenker, *Chem. Phys. Lett.* **110**, 351 (1984).
- ³¹J. C. Barthelat, B. S. Roch, G. Trinquier, and J. Satge, *J. Am. Chem. Soc.* **102**, 4080 (1980).
- ³²G. Olbrich, *Chem. Phys. Lett.* **73**, 110 (1980).
- ³³D. J. Clouthier and J. Karolczak, *J. Chem. Phys.* **94**, 1 (1991).
- ³⁴J. Karolczak, D. L. Joo, and D. J. Clouthier, *J. Chem. Phys.* **99**, 1447 (1993).
- ³⁵J. Karolczak and D. J. Clouthier, unpublished.
- ³⁶J. Karolczak and D. J. Clouthier, *Chem. Phys. Lett.* **201**, 409 (1993).

- ³⁷J. Karolczak, D. J. Clouthier, and R. H. Judge, to be published.
- ³⁸J. Karolczak, Q. Zhuo, D. J. Clouthier, W. M. Davis, and J. D. Goddard, *J. Chem. Phys.* **98**, 60 (1993).
- ³⁹J. Karolczak, R. S. Grev, and D. J. Clouthier, *J. Chem. Phys.* **101**, 891 (1994).
- ⁴⁰S. Sharpe and P. Johnson, *Chem. Phys. Lett.* **107**, 35 (1984).
- ⁴¹C. Jouvét, C. Lardeux-Dedonder, and D. Solgardi, *Chem. Phys. Lett.* **156**, 569 (1989).
- ⁴²C. S. Feigerle and J. C. Miller, *J. Chem. Phys.* **90**, 2900 (1989).
- ⁴³S. K. Bramble and P. A. Hamilton, *Chem. Phys. Lett.* **170**, 107 (1990).
- ⁴⁴C. Styger and M. C. L. Gerry, *Chem. Phys. Lett.* **188**, 213 (1992).
- ⁴⁵S. K. Bamble and P. A. Hamilton, *Meas. Sci. Technol.* **2**, 916 (1991).
- ⁴⁶M. L. Rutherford, D. J. Clouthier, and F. J. Holler, *Appl. Spectrosc.* **43**, 532 (1989).
- ⁴⁷T. E. Sharp and H. M. Rosenstock, *J. Chem. Phys.* **41**, 3453 (1964).
- ⁴⁸B. O. Roos, *Adv. Chem. Phys.* **69**, 399 (1987).
- ⁴⁹(a) S. J. Huzinaga, *J. Chem. Phys.* **42**, 1293 (1965); (b) T. H. Dunning, *J. Chem. Phys.* **55**, 716 (1971).
- ⁵⁰T. H. Dunning, *J. Chem. Phys.* **66**, 1382 (1977).
- ⁵¹(a) J. Almlof and P. R. Taylor, *J. Chem. Phys.* **86**, 4070 (1987); (b) J. Almlof, T. Helgaker, and P. R. Taylor, *J. Phys. Chem.* **92**, 3029 (1988); (c) J. Almlof and P. R. Taylor, *J. Chem. Phys.* **92**, 551 (1990); (d) J. Almlof and P. R. Taylor, *Adv. Quantum Chem.* **22**, 301 (1991).
- ⁵²P.-O. Widmark, P.-A. Malmqvist, and B. O. Roos, *Theor. Chim. Acta* **77**, 291 (1990).
- ⁵³H. Partridge, *J. Chem. Phys.* **90**, 1043 (1989).
- ⁵⁴C. W. Bauschlicher, Jr., S. R. Langhoff, and P. R. Taylor, *Adv. Chem. Phys.* **77**, 103 (1990).
- ⁵⁵(a) J. E. Rice and N. C. Handy, *Chem. Phys. Lett.* **107**, 365 (1984); (b) C. Winter and P. Millie, *Chem. Phys.* **174**, 177 (1993).
- ⁵⁶J. S. Francisco, R. Barnes, and J. W. Thoman, Jr., *J. Chem. Phys.* **88**, 2334 (1988).
- ⁵⁷C. E. Moore, *Atomic Energy Levels*, NSRDS-NBS Vol. 35 (US GPO, Washington, 1971).
- ⁵⁸R. S. Grev, C. L. Janssen, and H. F. Schaefer, *J. Chem. Phys.* **95**, 5128 (1991).
- ⁵⁹(a) B. Ruscic, M. Schwartz, and J. Berkowitz, *J. Chem. Phys.* **92**, 1865 (1990); *ibid.* **92**, 6338 (1990).
- ⁶⁰(a) M. J. Almond, A. M. Doncaster, P. N. Noble, and R. Walsh, *J. Am. Chem. Soc.* **104**, 4717 (1982); (b) P. N. Noble and R. Walsh, *Int. J. Chem. Kinet.* **15**, 547 (1983).
- ⁶¹M. Fukushima and K. Obi, *J. Chem. Phys.* **100**, 6221 (1994).
- ⁶²I. Dubois, *Can. J. Phys.* **46**, 2485 (1968).
- ⁶³J. W. Thoman, Jr., J. I. Steinfeld, R. I. McKay, and A. E. W. Knight, *J. Chem. Phys.* **86**, 5909 (1987).
- ⁶⁴R. I. McKay, A. S. Uichanco, A. J. Bradley, J. R. Holdsworth, J. S. Francisco, J. I. Steinfeld, and A. E. W. Knight, *J. Chem. Phys.* **95**, 1688 (1991).
- ⁶⁵C. G. Stevens and J. C. D. Brand, *J. Chem. Phys.* **58**, 3324 (1973).
- ⁶⁶C. M. Van Zoeren, J. W. Thoman, Jr., J. I. Steinfeld, and M. W. Rainbird, *J. Phys. Chem.* **92**, 9 (1988).